Published in "The Journal of Organic Chemistry 7(14): 5312 -5319, 2006"
which should be cited to refer to this work.

http://doc.rero.ch

Anthralin: Primary Products of Its Redox Reactions

Malgorzata Czerwinska, Adam Sikora, Piotr Szajerski, Jacek Zielonka, Jan Adamus, and Andrzej Marcinek*

Institute of Applied Radiation Chemistry, Technical University, 90-924 Lodz, Poland

Krzysztof Piech, Pawel Bednarek, and Thomas Bally*

Department of Chemistry, University of Fribourg, CH-1700 Fribourg, Switzerland

marcinek@p.lodz.pl; thomas.bally@unifr.ch

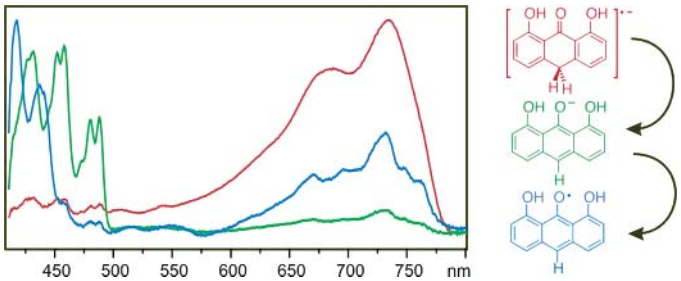

One-electron reduction significantly enhances the ability of anthralin, **1**, to act as a hydrogen atom donor. On annealing of an MTHF glass in which the radical anion of anthralin, $\mathbf{1}^{\bullet-}$, is generated radiolytically, this species decays mainly by loss of $H^{\bullet}$ to give the anthralyl anion, $\mathbf{2}^{-}$. On the other hand, radicals formed on radiolysis of matrices that are suitable for the generation of radical anions or cations are capable to abstract $H^{\bullet}$ from anthralin to give the anthralyl radical, $\mathbf{2}^{\bullet}$. Both $\mathbf{2}^{-}$ and $\mathbf{2}^{\bullet}$ are obtained simultaneously by mesolytic cleavage of the radical anion of the anthralin dimer. Contrary to general assumptions, the anthralyl radical is found to be much more reactive toward oxygen than the anion. All intermediates are characterized spectroscopically and by reference to quantum chemical calculations. Attempts to generate the radical cation of anthralin by X-irradiation of an Ar matrix containing anthralin led also to significant formation of its radical anion, i.e., anthralin acts apparently as an efficient electron trap in such experiments.

1. Introduction

Anthralin (**1**) (1,8-dihydro-9-anthrone or 1,8-dihydro-9,10*H*-anthracenone) is one of the most effective drugs for topical treatment of psoriasis, a common skin disease. This synthetic substitute of the natural product, chrysarobin, targets both the inflammatory and hyperproliferative aspects of the disease. Despite the fact that this drug has been successfully used for over 70 years, the accurate mechanism of the action of anthralin has not been elucidated.[1−5]

The therapeutic action of anthralin is related to its interaction with DNA and the inhibition of enzymes associated with cell proliferation and inflammation or lipid peroxidation and the destruction of membrane lipids.[1−7] There is growing evidence that these biological effects are related to redox reactions of anthralin resulting in the formation of anthralyl radicals[8−15] and the production of reactive oxygen species (ROS).[4,5,16,17] These species may be also responsible for undesired side effects of anthralin, such as skin irritation and staining.[6]

(1) Ashton, O. I.; Andre, P.; Lowe, N. J.; Whitefield, M. *J. Am. Acad. Dermatol.* **1983**, *9*, 173.
(2) Kemeny, E.; Ruzicka, T.; Braun-Falco, O. *Skin Pharmacol.* **1990**, *3*, 1.
(3) van de Kerkhof, P. M. *Eur. J. Dermatol.* **1991**, *1*, 79.
(4) Müller, K. *Biochem. Pharmacol.* **1997**, *53*, 1215.
(5) Müller, K. *Gen. Pharmac.* **1996**, *27*, 1325.
(6) Müller, K.; Gürster, D. *Biochem. Pharmacol.* **1993**, *46*, 1695.
(7) Wiegrebe, W.; Müller, K. *Skin Pharmacol.* **1995**, *8*, 1.
(8) Martinmaa, J.; Vanhala, L.; Mustakallio, K. K. *Experientia* **1978**, *34*, 872.
(9) Davies, A. G.; Hawari, J. A. A.; Whitefield, M. *Tetrahedron Lett.* **1983**, *24*, 4465.
(10) Mustakallio, K. K.; Martinmaa, J.; Vilvara, R.; Hamekoski, J. *Med. Biol.* **1984**, *62*, 155.
(11) D'Ischia, M.; Prota, G. *Gazz. Chim. Ital.* **1985**, *115*, 511.
(12) Shroot, B.; Brown, C. *Arzneim. Forsch.* **1986**, *36*, 1253.
(13) Fuchs, J.; Packer, L. *Invest. Dermatol.* **1989**, *92*, 677.
(14) Lambelet, P.; Ducret, F.; Löliger, J.; Maignan, J.; Reichert, U.; Shroot, B. *Free Radic. Biol. Med.* **1990**, *9*, 183.
(15) Hayden, P. J.; Free, K. E.; Chignell, C. F. *Mol. Pharmacol.* **1994**, *46*, 186.

SCHEME 1. Compounds Potentially Involved in the Redox Reactions of Anthralin[a]

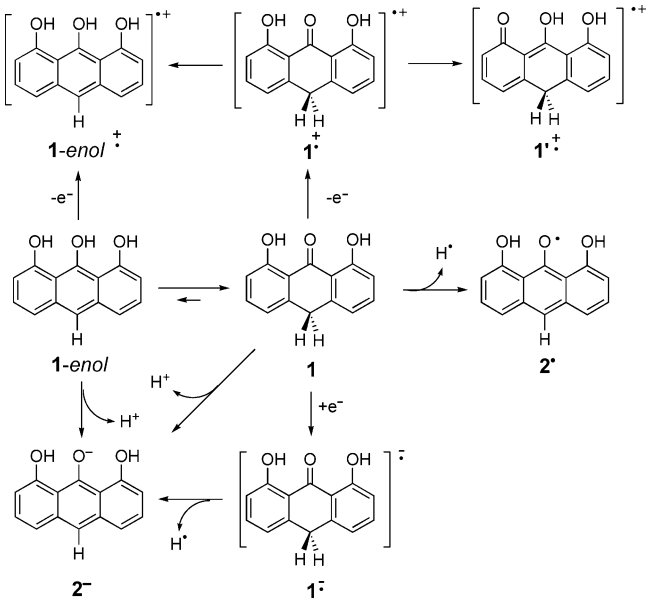

[a] Species **2** lacks a hydrogen atom compared to species **1**.

Studies of the redox reactions of anthralin may be helpful in elucidating its therapeutic action. In the present study, the transient species generated upon one-electron reduction and oxidation of anthralin are identified and characterized for the first time. These studies reveal that upon reduction anthralin spontaneously loses a proton to yield the anthralyl anion, **2**$^-$ (the enolate of 1,8,9-trihydroxyanthracene), while the corresponding radical, **2**$^\bullet$ (1,8-dihydro-9-anthron-10-yl), is formed directly from the neutral anthralin by hydrogen atom abstraction rather than by oxidation of the anthralyl anion (cf. Scheme 1).

It has been claimed that anthralin reacts with oxygen to yield the superoxide radical anion, but there is strong evidence that auto-oxidation of anthralin can only occur in its enol form (**1**-*enol*) or in the anthralyl anion **2**$^-$ (Scheme 1).[4,5,17] Therefore, it was proposed that these two species react with oxygen, producing superoxide and the radical cation of **1**-*enol* or the anthralyl radical, **2**$^\bullet$, respectively. The role of **2**$^\bullet$ in the therapeutic process is not known, but it is often questioned because **2**$^\bullet$ is a particularly stable radical, as shown by its low reactivity toward oxygen or vitamin E.[18]

In this paper, we explore a different pathway for the generation of **2**$^\bullet$: we have found that one-electron reduction of **1** or its 10,10′-dehydrodimer **(2)**$_2$ (1,8,1′,8′-tetrahydroxy-10,-10′-bisanthrone) leads to concomitant formation of **2**$^-$ and **2**$^\bullet$ under the same experimental conditions (Scheme 2) and thus allows for the direct comparison of their reactivity toward oxygen.

The photochemistry of anthralin is also of considerable interest since UV radiation is often used as an adjunct to anthralin therapy, although exposure of skin treated with the drug to light causes irritation and erythema. This sensitivity to light and oxygen indicates that some photochemically generated

SCHEME 2. Reductive Cleavage of the Dehydro Dimer of Anthralin

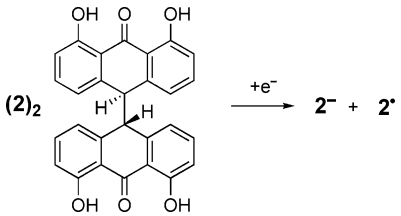

intermediates may be involved in the mode of action of the drug, among them the primary products of electron-transfer reactions, i.e., radical ions or neutral radicals which we characterize in this work.

2. Results and Discussion

Anthralin Radical Anion. Anthralin (**1**) is poorly soluble in aqueous solutions, alcohols, and in the organic solvents used commonly to form low-temperature glasses. In experiments where radical ions are generated by radiolytic reduction or oxidation in solid matrices, the concentration of solute molecules must be at least 10^{-3} M to ensure efficient scavenging of the initially generated electrons or holes. Poor solubility of the solute, even if it has a low ionization potential or a high electron affinity, may therefore represent a significant obstacle.

On the other hand, in alkaline aqueous or alcoholic solutions, or in polar solvents such as acetonitrile, anthralin is deprotonated, at least partially, to **2**$^-$. The pK_a value of anthralin was found by titration in aqueous buffer solutions to be 9.5.[19,20] Although the concentration of **2**$^-$ must therefore be very limited under physiological conditions, there is conclusive evidence for the formation of superoxide during the auto-oxidation of anthralin anion.[17,21] In contrast to **2**$^-$ or **1**(*enol*), both of which are susceptible to auto-oxidation, the keto form of anthralin is not; hence, the transient products of redox reactions of **1** in its keto form have not been identified to date. We start out by presenting the characteristics of the radical anion of **1**.

The optical spectrum obtained on pulse radiolysis of a solution of anthralin in a glass of deoxygenated 2-methyltetrahydrofuran (MTHF) at 77 K[22] (red trace in Figure 1A) is composed of a strong band peaking at 740 nm (followed by two members of a vibrational progression of ca. 980 cm^{-1}), accompanied by some weaker features at shorter wavelengths. As **1** exists exclusively in its keto form (which shows a strong structureless band at 356 nm) in MTHF, the above spectrum must be ascribed to **1**$^{\bullet-}$. According to our calculations, the slightly bent keto form of **1**$^{\bullet-}$ is more stable than its planar enol form by nearly 33 kcal/mol; i.e., the order of keto/enol stability of **1** is not inverted on reduction. Hydrogen atom transfer from one of the hydroxyl groups to the central carbonyl group, as it had been observed to occur in the excited state of **1**,[23,24] is also unfavorable in **1**$^{\bullet-}$

(16) Müller, K.; Kappus, H. *Biochem. Pharmacol.* **1988**, *37*, 4277.
(17) Bruce, J. M.; Kerr, C. W.; Dodd, N.; J. F. *J. Chem. Soc., Faraday Trans. 1* **1987**, *83*, 85.
(18) Bruce, J. M.; Dodd, N. J. F.; Gorman, A. A.; Hamblett, I.; Kerrr, C. W.; Lambert, C.; McNeeney, S. P. *Photochem. Photobiol.* **1990**, *52*, 345.
(19) Müller, K.; Kanner, R. C.; Foote, C. S. *Photochem. Photobiol.* **1990**, *52*, 445.
(20) Sa e Melo, T.; Dubertret, L.; Prognon, P.; Gond, A.; Mahuzier, G.; Santus, R. *J. Invest. Dermatol.* **1983**, *80*, 1.
(21) Müller, K.; Wiegrebe, W.; Younes, M. *Arch. Pharm. (Weinheim)* **1987**, *320*, 59.
(22) Shida, T. *Electronic Absorption Spectra of Radical Ions*; Elsevier: Amsterdam, 1988.
(23) Andersen, K. B.; Spanget-Larsen, J. *Spectrochim. Acta* **1997**, *53 A*, 2615.
(24) Moller, S.; Andersen, K. B.; Spanget-Larsen, J.; Waluk, J. *Chem. Phys. Lett* **1998**, *291*, 51.

http://doc.rero.ch

http://doc.rero.ch

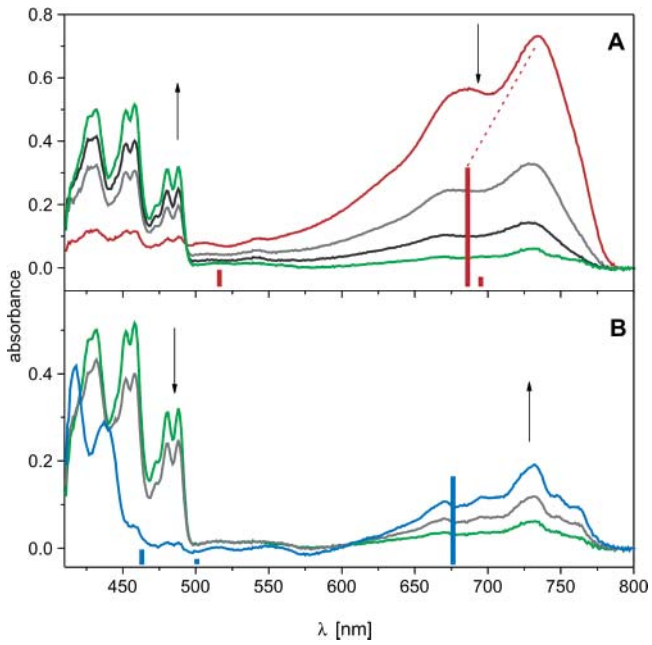

FIGURE 1. (A) Red trace: electronic absorption spectrum obtained on radiolysis of anthralin **1** embedded in an MTHF glass at 77 K (0.02 M solution, radiation dose 2.5 kGy, optical path 2 mm). Gray and black traces: decay of $\mathbf{1}^{\bullet-}$ and buildup of $\mathbf{2}^{-}$ (bands at 400−500 nm) on annealing at 90−95 K. (B) Spectral changes observed on further annealing of an MTHF glass already containing $\mathbf{2}^{-}$ (green spectrum) at 95−100 K. The final blue spectrum is asssigned to $\mathbf{2}^{\bullet}$ (see text). The red bars in (A) and the blue bars in (B) represent the results of the TD-DFT calculations for $\mathbf{1}^{\bullet-}$ (Table 1) and $\mathbf{2}^{\bullet}$ (Table 3), respectively.

TABLE 1. Excited States and Electronic Transitions of $\mathbf{1}^{\bullet-}$ by TD-B3LYP/6-31+G* Calculations

state	λ_{max}/nm	$f \times 10^2$	excitations[a]
1^2B_1			$(7b_1)^1$
2^2B_1	695	1.01	$7b_1 \rightarrow 8b_1$
1^2A_2	686	11.91	$7b_1 \rightarrow 5a_2$
1^2A_1	669	0.28	$7b_1 \rightarrow 28a_1$
1^2B_2	611	0	$7b_1 \rightarrow 23b_2$
2^2A_1	532	0	$7b_1 \rightarrow 29a_1$
2^2A_2	516	3.41	$7b_1 \rightarrow 6a_2$

[a] In terms of the MOs shown in Figure S1 of the Supporting Information; the listed excited configurations have coefficients >0.9 in the CIS-type wave function. No intense transitions were predicted between 500 and 350 nm.

($\Delta H = +6.4$ kcal/mol). The observed spectrum is in accord with the results of TD-DFT calculations (Table 1) which predict a strong absorption with λ_{max}=686 nm, preceded by a 10 times weaker one at 695 nm (which could be responsible for the weak long-wavelength shoulder).

The next possibly palpable transition is predicted at 516 nm, i.e., where the experimental spectrum is empty, but it is unclear whether gas-phase TD-DFT calculations are capable of predicting the positions of higher lying excited states of radical anions (which are usually dissociative in vacuo) in condensed phase with any accuracy, especially if these states involve σ^* MOs. It is, however, interesting to note that all electronic transitions of $\mathbf{1}^{\bullet-}$ in the visible range involve excitation from the singly occupied MO (SOMO, $7b_1$) to higher lying virtual orbitals (including a_1 and b_2 σ^*-MOs) and that excitations *into* the SOMO do not contribute to the spectrum of $\mathbf{1}^{\bullet-}$ predicted by the TD-DFT method.

Experiments conducted with initial concentrations of **1** ranging from 5×10^{-3} to 7.5×10^{-2} M (but with the same radiation dose) showed that the yield of $\mathbf{1}^{\bullet-}$ is independent of the concentration of **1** and that no traces of unscavenged, solvated electrons (λ_{max}= 1200 nm) remain in that concentration range.

TABLE 2. Excited States and Electronic Transitions of $\mathbf{2}^{-}$ by TD-B3LYP/6-31+G* Calculations

state	λ_{max}/nm	$f \times 10^2$	excitations[a]
1^1A_1			$(6b_1)^2$
2^1A_1	433	7.36	$6b_1 \rightarrow 7b_1$
1^1B_1	387	<0.01	$6b_1 \rightarrow 28a_1$
1^1A_2	369	0	$6b_1 \rightarrow 23b_2$
1^1B_2	359	25.15	$6b_1 \rightarrow 5a_2$
2^1B_1	336	0.09	$6b_1 \rightarrow 29a_1$
3^1B_1	311	0.34	$6b_1 \rightarrow 30a_1$
2^1A_2	310	0	$6b_1 \rightarrow 24b_2$
2^1B_2	308	6.54	$6b_1 \rightarrow 6a_2$

[a] In terms of the π-MOs shown in Figure S2 of the Supporting Information (the a_1 and b_2 σ^*-MOs are very similar to those shown in Figure S1 of the Supporting Information); the listed excited configurations have coefficients >0.9 in the CIS-type wave function.

TABLE 3. Excited States and Electronic Transitions of $\mathbf{2}^{\bullet}$ by TD-B3LYP/6-31G* Calculations

state	λ_{max}/nm	$f \times 10^2$	excitations[a]
1^2B_1			$(6b_1)^1$
1^2A_2	676	8.86	$4a_2 \rightarrow 6b_1$
2^2B_1	549	<0.01	$5b_1 \rightarrow 6b_1$
2^2A_2	501	0.58	$3a_2 \rightarrow 6b_1$
1^2B_2	468	0	$22b_2 \rightarrow 6b_1$
3^2B_1	463	1.56	$6b_1 \rightarrow 7b_1$

[a] In terms of the MOs shown in Figure S2 in the Supporting Information; the listed excited configurations have coefficients >0.9 in the CIS-type wave function. No intense transitions are predicted betweeen 450 and 350 nm.

The inhibitory effect of the rigid matrix on intermolecular processes gradually withers on annealing a MTHF matrix slightly above its glass transition temperature, ca. 90 K. If this is done, a new system of bands with twin peaks centerd at 430, 455, and 485 nm arises at the expense of the bands of $\mathbf{1}^{\bullet-}$ (see Figure 1A). By comparison with spectra of **1** taken in DMF or in alkaline MeOH solution,[25,26] as well as with the TD-DFT calculations in Table 2, we assign this new spectrum to $\mathbf{2}^{-}$.

Unfortunately, the strongest band of this anion (observed at 392 nm in DMF[25] and predicted at 359 nm in vacuo) is not visible under our experimental conditions because it is obscured by strong absorptions of **1**. The observed band system appears to be due to a single electronic transition (HOMO → LUMO) showing vibrational progressions of ca. 1330 and 310 cm^{-1} which had not been revealed by the previous solution spectra.[25,26] The absorptions of $\mathbf{2}^{-}$ grow until the bands of $\mathbf{1}^{\bullet-}$ have completely decayed.

Prolonged annealing of the matrix at elevated temperatures (above 100 K) leads to the decay of $\mathbf{2}^{-}$ and the appearance of a new, different band system at 600−800 nm (λ_{max} = 730 nm, Figure 1B) which we assign to the neutral radical $\mathbf{2}^{\bullet}$ by comparison to the known spectrum of this species in solution[18,27] and the results of the TD-DFT calculations in Table 3. These show again that the observed band system must be due to a single electronic transition (which is predicted ca. 0.14 eV too

(25) Sellmer, A.; Terpetschnig, E.; Wiegrebe, W.; Wolfbeis, O. S. *J. Photochem. Photobiol. A: Chem.* **1998**, *116*, 39.
(26) Dabestani, R.; Hall, R. D.; Sik, R. H.; Chignell, C. F. *Photochem. Photobiol.* **1990**, *52*, 961.
(27) Bruce, J. M.; Gorman, A. A.; Hamblett, I.; Kerr, C. W.; Lambert, C.; McNeeney, S. P. *Photochem. Photobiol.* **1989**, *49*, 439.

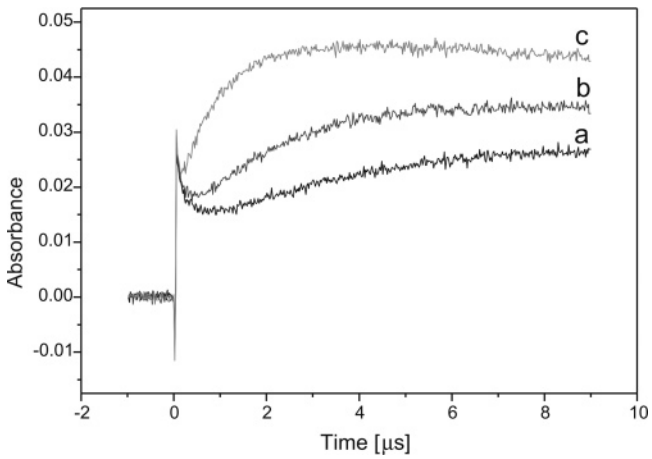

FIGURE 2. Kinetic traces of the changes in absorbance at 680 nm of the transient species generated by pulse radiolysis of (a) 0.005 M, (b) 0.01 M, and (c) 0.05 M solutions of **1** in deareated MTHF at 25 °C (radiation dose 65 Gy, optical path 10 mm).

high in energy), this time from the highest doubly occupied MO to the SOMO.

TD-DFT predicts weak transitions at ca. 500 and 460 nm which could give rise to the little bumps in that region, but no further intense transitions down to 350 nm. Thus, the band at 440 nm, which later continues to grow at the expense of the bands of $\mathbf{2}^{\bullet}$, is not due to $\mathbf{2}^{\bullet}$. Bruce et al. have previously suggested[18] that this band could be due to a tautomeric form of the dimer $\mathbf{(2)_2}$, formed upon radical dimerization, but it could also be due to secondary radicals.[13−15] As will be discussed in the following section, we also found that, upon reduction, $\mathbf{(2)_2}$ undergoes spontaneous fragmentation to $\mathbf{2}^{\bullet}$ and $\mathbf{2}^{-}$, which therefore constitutes an independent route for the formation of these species in an MTHF glass.

Formation of $\mathbf{2}^{-}$ from $\mathbf{1}^{\bullet-}$ requires the detachment of a hydrogen atom from the C-10 position,[25] which may be a facile process if a suitable acceptor is available. Possible candidates are neutral solvent or solute molecules or radicals formed upon matrix irradiation. As the yield of $\mathbf{2}^{-}$ depends only on the initial yield of $\mathbf{1}^{\bullet-}$ which in turn does *not* depend on the concentration of **1** (see above), we assume that **1** does not serve as a hydrogen atom acceptor. Thus, hydrogen atoms must be transferred to the solvent molecules or onto the byproducts of radiolysis, the concentration of which depends only on the irradiation dose.

The fact that the formation of $\mathbf{2}^{\bullet}$ occurs at the expense of $\mathbf{2}^{-}$ seems to indicate that the process is a simple auto-oxidation of $\mathbf{2}^{-}$, as it has been shown to occur in reactions with stable radicals such as nitroxides.[17,21,28] It could be that byproducts of the radiolysis act as electron acceptors in frozen MTHF. However, experiments conducted with different initial concentrations of **1**, both under matrix conditions and in solution (see Figure 2), show an increase of the yield of $\mathbf{2}^{\bullet}$ and the rate of its formation with the concentration of **1**, in contrast to $\mathbf{2}^{-}$ (see above).

As both $\mathbf{1}^{\bullet-}$ and $\mathbf{2}^{\bullet}$ absorb around 700 nm, the initial decay seen in the kinetic traces in Figure 2 reflects the decay of $\mathbf{1}^{\bullet-}$, but on a longer time scale the formation of $\mathbf{2}^{\bullet}$ dominates the absorption at 680 nm. From this part of the trace, pseudo-first-order rate constants for the formation of $\mathbf{2}^{\bullet}$ can be obtained from which second-order rate constants of ca. 10^8 M^{-1} s^{-1} can be estimated. As the yield of $\mathbf{2}^{-}$ and the rate for its decay do not depend on the initial concentration of **1**, the parallel decay of the anion and the growth of the radical absorption (Figure 1B) should be assigned to two independent intermolecular reactions.

Although MTHF is an aprotic solvent, the positive ions, $C_5H_{11}O^+$, that are generated on irradiation of the matrix (reaction 5 in the Experimental Section) may act as proton donors. A good example of this is the well-documented formation of ketyl radicals on radiolysis and subsequent annealing of MTHF matrices containing benzophenone and acetophenone.[22,29] The same could happen to $\mathbf{2}^{-}$ which would then re-form **1** (reaction 1).

$$\mathbf{2}^{-} + C_5H_{11}O^+ \rightarrow \mathbf{1} + C_5H_{10}O \qquad (1)$$

$$\mathbf{1} + C_5H_9O^{\bullet} \rightarrow \mathbf{2}^{\bullet} + C_5H_{10}O \qquad (2)$$

On the other hand, because of the high stability of the radical $\mathbf{2}^{\bullet}$, anthralin itself may act as a hydrogen atom donor in reactions with less stable radicals, a process which has been amply documented.[16,18,27,30] In the present case, $C_5H_9O^{\bullet}$, the other product that is formed in irradiation of solid MTHF (cf. reaction 5 in the Experimental Section), may play this role and react with **1** to form $\mathbf{2}^{\bullet}$ (reaction 2). This process would explain the dependence of the rate of formation of $\mathbf{2}^{\bullet}$ on the concentration of **1** (see Figure 2). On the other hand, the yield of $\mathbf{2}^{\bullet}$ increases also with the irradiation dose, i.e., when more $C_5H_9O^{\bullet}$ radicals are formed. According to our calculations, reaction 2 is exothermic by 21.1 kcal/mol. This "repair" reaction of anthralin with free radicals may be responsible for the antioxidant properties of this compound.

If reaction 2 is responsible for the formation of $\mathbf{2}^{\bullet}$ in the cryogenic experiments, it is interesting to compare the hydrogen atom donor properties of anthralin itself and its radical anion. Addition of one electron to the molecule appears to significantly increase the propensity for hydrogen atom detachment, as seen by the difference in the rates for both processes under matrix conditions (hydrogen atom transfer from $\mathbf{1}^{\bullet-}$ precedes that from **1**). According to DFT calculations, a good part of the spin in $\mathbf{1}^{\bullet-}$ is located at C10 (Mulliken spin population = 0.28), which facilitates abstraction of one of the hydrogen atoms attached to this carbon atom. Hence, $\mathbf{1}^{\bullet-}$ may react with MTHF, whereas **1** requires species of higher hydrogen atom affinity, such as $C_5H_9O^{\bullet}$.

Anthralin Dimer Radical Anion. We have shown above that adding an electron to anthralin facilitates cleavage of the C(10)−H bond. This finding led us to expect that reduction of the anthralin dimer, $\mathbf{(2)_2}$, will lead to its spontaneous cleavage. Such so-called mesolytic fragmentation processes[31] are more commonly activated by *removal* of an electron, thus providing a useful method of breaking bonds that are quite strong in neutral substrates,[31,32] but there are also some examples of fragmentations following *attachment* of an electron.[33] According to DFT calculations, mesolytic fragmentation of the radical anion of $\mathbf{(2)_2}$ to $\mathbf{2}^{-}$ and $\mathbf{2}^{\bullet}$ is exothermic by 5.7 kcal/mol in the gas phase

(28) Pecar, S.; Schara, M.; Muller, K.; Wiegrebe, W. *Free Rad. Biol. Med.* **1995**, *18*, 459.

(29) Hayon, E.; Ibata, T.; Lichtin, N. N.; Simic, M. *J. Phys. Chem.* **1972**, *76*, 2072.

(30) Müller, K.; Leukel, P.; Ziereis, K.; Gawlik, I. *J. Med. Chem.* **1994**, *37*, 1660.

(31) Mazlak, P. *Top. Curr. Chem.* **1993**, *168*, 1.

(32) Rogowski, J.; Zielonka, J.; Marcinek, A.; Gebicki, J.; Bednarek, P. *J. Phys. Chem. A.* **2003**, *107*, 810.

http://doc.rero.ch

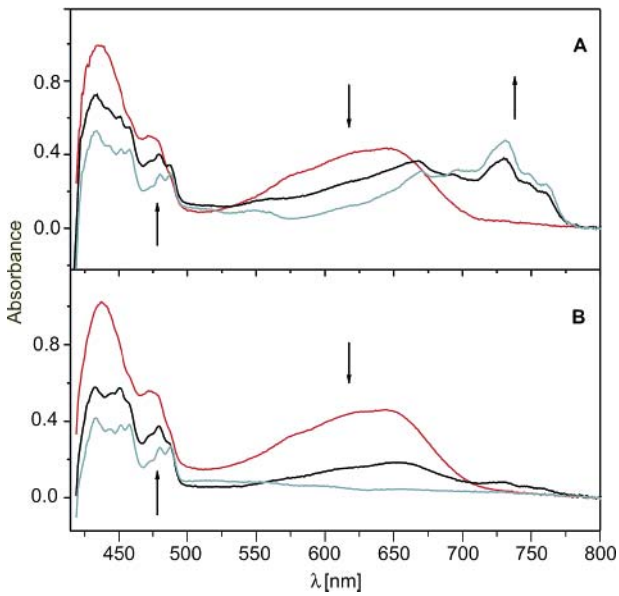

FIGURE 3. (A) Red spectrum: Electronic absorption spectrum obtained after radiolysis of a frozen MTHF saturated with anthralin dimer, $\mathbf{(2)_2}$ (<0.005 M, deoxygenated solution, radiation dose 4.1 kGy, sample thickness 2 mm) at 77 K. Black and gray traces: spectral changes observed upon annealing of the above matrix at 90−95 K. (B) Same as A, but starting with a solution that was saturated with O_2 before freezing (note that the initial spectrum is not affected by the presence of O_2).

(and probably more so in MTHF because of stronger solvation of the more localized monomer anion).

The electronic absorption spectrum obtained upon reduction of $\mathbf{(2)_2}$ in MTHF at 77 K is presented in Figure 3 (red spectrum). It is composed of a broad absorption band peaking at 650 nm and a more intense one at 445 nm with a weak shoulder at 470 nm. We assign this spectrum to the primary radical anion, $\mathbf{(2)_2}^{\bullet-}$, although substantiating this assignment by calculations is not a trivial matter because it is unclear whether solvation favors a situation where charge and spin are localized in one of the two anthralin moieties or whether they are delocalized over both, even in MTHF. DFT calculations invariably predict the latter because it is impossible to enforce a localization of spin and charge with such methods.[34] It is also unclear whether the C−C σ-bond linking the two halves of $\mathbf{(2)_2}^{\bullet-}$ is still intact or whether the red spectrum in Figure 3 is due to a π-complex between $\mathbf{2}^-$ and $\mathbf{2}^\bullet$. In any event, this species is stable at 77 K because its dissociation is inhibited by the rigidity of the MTHF matrix. However, slight softening of the matrix by annealing it to 90 K leads to the disappearance of the red spectrum, a decay which is accompanied by the rise of the sharp bands at 440−500 nm of $\mathbf{2}^-$ and the structured band system at 500−800 nm of $\mathbf{2}^\bullet$ (gray and black traces in Figure 3A).

Both species are formed simultaneously and with similar rates. Their decay upon further annealing of the matrix is also similar. If $\mathbf{2}^-$ were oxidized to $\mathbf{2}^\bullet$, some differences in the decay kinetics of both species should occur. Their parallel disappearance indicates, however, independent decay paths which are triggered under the same conditions of softening the matrix.

Saturating the MTHF solution with oxygen before freezing does not affect the yield of the primary radical anion or of the anion $\mathbf{2}^-$ formed on its fragmentation, whereas $\mathbf{2}^\bullet$ is effectively quenched (Figure 3B). This contrasts with the general assumption that, due to its stability and inertness toward oxygen, $\mathbf{2}^\bullet$ should be discounted as an important intermediate in the mode of action of anthralin as an antipsoriatic drug,[4,18] in contrast to $\mathbf{2}^-$, the formation of which was considered as a first step toward generation of reactive oxygen species. From the above experiments, it is, however, clear that, in actual fact, the anion is even more inert toward oxygen than the radical. Therefore, the direct autoxidation of $\mathbf{2}^-$ through reaction with O_2 (to form $O_2^{\bullet-}$) is probably too slow to be effective in the absence of catalysts such as iron or copper.[4,5,35]

If anthralin itself is reduced in O_2-saturated MTHF matrices the radical absorption is also absent from the spectra at any stage of the annealing process (in contrast to the spectra presented in Figure 1B) although the decay of the anion $\mathbf{2}^-$ is not affected. As dimerization of radicals under these experimental conditions is impeded, reaction with oxygen takes over, leading probably to the formation of the anthralyl peroxy radical.

Attempts To Generate the Anthralin Radical Cation. Radicals such as $\mathbf{2}^\bullet$ may also be formed by way of *radical cations* which often undergo facile deprotonation.[36] Therefore, we decided to look also at the oxidation of **1**. We were able to dissolve enough **1** in the Freon mixture to get a strong absorption at <300 nm. However, γ-irradiation of the glass formed from this solution only led to a broad band peaking at ca. 600 nm (dashed line a in Figure 4) which usually occurs when no species that are more easily oxidizable than the Freons are available to trap the positive charges. This band can be readily bleached (Figure 4b), but still no absorptions that could be attributed to $\mathbf{1}^{\bullet+}$ are revealed. In contrast, a solution of similar concentration of **1** in an MTHF glass exposed to the same conditions of irradiation resulted in spectrum c in Figure 4, which is almost identical to that obtained after pulse radiolysis in the same solvent (Figure 1A, red spectrum).

Because we were not sure whether our failure to observe $\mathbf{1}^{\bullet+}$ was due to an insufficient concentration of **1** in the Freon mixture, we resorted to the Ar matrix technique for further experiments. Thus, we fed **1** into a stream of Ar/N_2 (10:1) doped with 0.1 mol % CH_2Cl_2 (which usually acts as an efficient electron scavenger) and deposited it on a CsI window held at 20 K. The resulting matrix was exposed to 90 min of X-irradiation, a procedure that usually results in the conversion of 10−15% of the neutral substrate to its radical cation (or secondary products thereof).[37]

To our surprise, the spectrum which we obtained by this procedure (Figure 4d, dashed line) looked, however, almost indistinguishable from that recorded in MTHF and attributed to the *radical anion*, $\mathbf{1}^{\bullet-}$. We had never before obtained a radical anion under such conditions, although previous work had indicated that it is possible to generate radical anions of species with high electron affinities in Ar matrices by X-irradiation if amines are added (as hole scavengers).[38] In an experiment where we doped the Ar matrix with DABCO instead of CH_2Cl_2, a very similar spectrum was obtained (the yield of the radical anion was slightly enhanced), except that the absorption rising

(33) Chanon, M.; Rajzmann, M.; Chanon, F. *Tetrahedron* **1990**, *46*, 6193.
(34) Bally, T.; Sastry, G. N. *J. Phys. Chem. A.* **1997**, *101*, 7923.
(35) Miller, D. M.; Buettner, G. R.; Aust, S. D. *Free Rad. Biol. Med.* **1990**, *8*, 95.
(36) Roth, H. D.; Weng, H.; Zhou, D.; Lakkaraju, P. S. *Acta Chim. Scand.* **1997**, *51*, 626.
(37) Bally, T. In *Reactive Intermediate Chemistry*; John Wiley & Sons: Hoboken, NJ, 2004; p 797.
(38) Gebicki, J.; Michl, J. *J. Phys. Chem.* **1988**, *92*, 6452.

http://doc.rero.ch

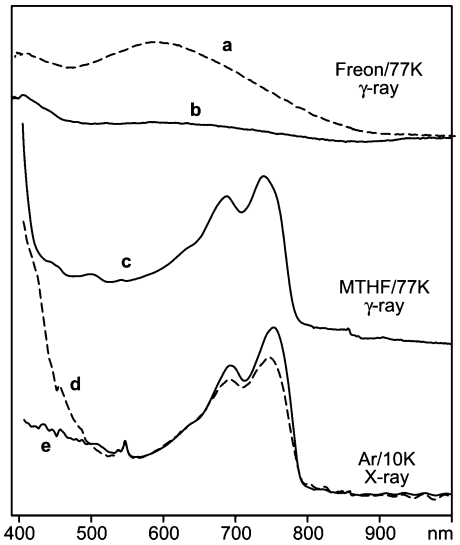

FIGURE 4. Difference spectra obtained on (a) ^{60}Co γ-radiolysis of a saturated solution of anthralin **1** in a Freon mixture (see the Experimental Section) at 77 K; (b) photolysis of the sample giving spectrum (a) at >600 nm; (c) ^{60}Co γ-radiolysis of a 10^{-3} M solution of **1** in MTHF at 77 K; (d, e) X-irradiation of a 12 K Ar matrix containing ca. 1 mol % of **1** and (d): a similar amount of CH_2Cl_2 (an efficient electron scavenger) or (e) a similar amount of DABCO (an efficient hole scavenger).

below 500 nm was missing (Figure 4e). At the same time, the formation of DABCO$^{\bullet+}$ (which has only a weak visible absorption) could be seen very clearly in the IR spectrum. Thus, we are forced to conclude that **1** is indeed a more efficient electron scavenger than CH_2Cl_2, i.e., that we have witnessed the efficient formation of a radical anion in an Ar matrix.[39,40]

The question remains whether, in the presence of CH_2Cl_2, **1**$^{\bullet+}$ is perhaps also formed, but does not manifest itself in the UV/Vis spectrum (unfortunately, the changes in the IR spectra are too weak to be diagnostically useful). To examine this possibility, we carried out some B3LYP/6-31G* calculations on **1**$^{\bullet+}$. The first thing to note from these results is that, similar to many other cases,[41,42] but in contrast to **1**$^{\bullet-}$, the order of stability of the keto and enol forms is inverted in **1**$^{\bullet+}$: While **1** is more stable than **1**(*enol*) by ca. 19 kcal/mol the radical cation of **1**(*enol*) is more stable than **1**$^{\bullet+}$ by 13.4 kcal/mol (this inversion of stabilities may explain why the enol form is susceptible to autoxidation, whereas the keto form is not). However, two reasons speak against the formation of **1**(*enol*)$^{\bullet+}$ under matrix conditions: first, the lowest energy pathway for the conversion of **1**$^{\bullet+}$ to its enol form (a sequence of five 1,2-H shifts, see Figure S4 in the Supporting Information) involves a barrier of over 40 kcal/mol which cannot be surmounted under

(39) Note that many radical anions were generated in Ar matrices and observed by the very sensitive technique of ESR spectroscopy (see, e.g.: Kasai, P. H. *Acc. Chem. Res.* **1971**, *4*, 329). However, to obtain transmission spectra, much higher concentrations of these species are required.

(40) To convince ourselves that such efficient formation of radical anions in Ar matrices doped with CH_2Cl_2 is indeed possible we carried out a similar set of experiments with *p*-benzoquinone. Indeed, upon X irradiation of such an Ar matrix containing this compound we obtained the characteristic spectrum of the corresponding radical anion.[22,38] In the IR spectrum, we witnessed the simultaneous formation of the radical cation of *p*-benzoquinone, a species which, to the best of our knowledge, has hitherto not been observed in condensed phase (Piech, K., Bally, T. Unpublished results).

(41) Gebicki, J.; Marcinek, A. In *General Aspects of Free Radical Chemistry*; Alfassi, Z. B., Ed.; Wiley: Chichester, 1999.

(42) Gebicki, J.; Bally, T. *Acc. Chem. Res.* **1997**, *30*, 477.

SCHEME 3. Tautomerization of the Radical Cation of Anthralin

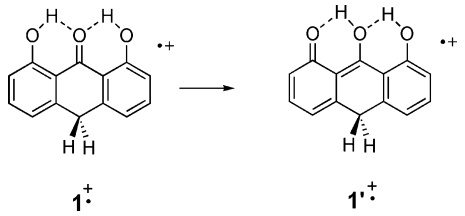

TABLE 4. Excited States and Electronic Transitions of 1′$^{\bullet+}$ by TD-B3LYP/6-31G* Calculations

state	λ_{max}/nm	$f \times 10^2$	leading excitations[a]
1^2A″			(10a″)^1
2^2A″	1405	0.31	9a″ → 10a″
2^2A′	813	<0.01	49a′ → 10a″
3^2A″	675	2.95	8a″ → 10a″
4^2A″	560	0.06	0.78 (10a″ → 11a″) −0.67 (9a″ → 11a″)
5^2A″	495	0.08	7a″ à 10a″
6^2A″	431	3.70	0.58 (10a″ → 11a″) + 0.67 (9a″ → 11a″)
7^2A″	411	8.25	0.78 (9a″ → 11a″)

[a] In terms of the MOs shown in Figure S3 in the Supporting Information; unless indicated, the listed excited configurations have coefficients >0.9 in the CIS-type wave function (note that the coefficients are not normalized in the G03 output).

these experimental conditions. Second, TD-DFT calculations for **1**(*enol*)$^{\bullet+}$ predict an intense band at 705 nm ($f = 0.107$) but no bands of similar intensity down to 300 nm, a prediction that is clearly incompatible with our observations.

On the other hand, it turns out that in the radical cation the quinoid tautomeric form **1′** (which is disfavored by ca. 26 kcal/mol in the neutral, due to loss of an aromatic ring, and by 6.4 kcal/mol in **1**$^{\bullet-}$) is only 0.8 kcal/mol less stable than **1**$^{\bullet+}$ by B3LYP/ 6-31G* and that the H-shift that leads to **1′**$^{\bullet+}$ is nearly barrierless (Scheme 3). Single-point calculations at the CCSD-(T) level predict **1′**$^{\bullet+}$ to be more stable than **1**$^{\bullet+}$ by 4.6 kcal/mol, so we believe that upon ionization, **1** tautomerizes spontaneously to the quinoid form **1′**.

According to TD-DFT calculations, **1′**$^{\bullet+}$ has two very weak NIR transitions, the first of which involves an electron transfer from the aromatic to the quinoid part of **1′**$^{\bullet+}$. Two bands of similar (medium) intensity are predicted at 675 and 431 nm, followed by a much stronger one at 411 nm (see Table 4). If the 675 nm band is hidden under the much more intense one of the (simultaneously formed) radical anion, then the latter two bands may account for the steep rise below 500 nm which disappears when the electron scavenger (CH_2Cl_2) is replaced by a hole scavenger (DABCO) in the Ar matrix experiments.

In conclusion, if **1** is oxidized under the conditions which usually lead to radical cations of substrates added to Ar matrices, then it will probably relax spontaneously to **1′**$^{\bullet+}$. However, the unmistakable presence of **1**$^{\bullet-}$ under these conditions suggests that **1** is a much better trap of the electrons that are liberated on X-irradiation of solid Ar than of the holes which are created at the same time. In fact, its electron-scavenging ability exceeds that of CH_2Cl_2.

As mentioned above, the solubility of anthralin in solvents such as 2-chlorobutane is too low for generation of any traces of the radical cation in this glassy matrix. However, upon softening of the irradiated 2-chlorobutane matrix containing soluble amounts of anthralin the formation of small amounts of radical **2**$^{\bullet}$ can be observed. Much better yields of this product are obtained if the experiment is done in ionic liquid glasses.

http://doc.rero.ch

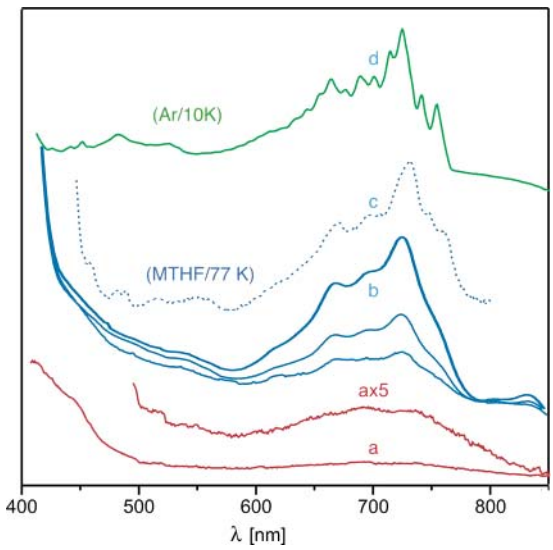

FIGURE 5. (a) Red trace: absorption spectrum obtained on radiolysis of **1** in an ionic liquid/$CHCl_3$ glass at 77 K (radiation dose 10 kGy, sample thickness 2 mm). Blue traces: spectral changes observed upon subsequent annealing of the matrix (trace b: final spectrum; c: spectrum of **2**• (reproduced from Figure 1); d: spectrum of **2**• obtained by depositing **(2)**$_2$ into an Ar matrix.

We have shown previously that these novel solvents, many of which form transparent glasses at 77 K,[23] can be used for generating radical ions by radiolysis and studying them by transmission spectroscopy. Recently, we found that the glass quality does not change upon addition of an organic component to the ionic liquid. For example, 1:1 mixtures of 1-butyl-3-methylimidazolium hexafluorophosphate and $CHCl_3$ form a transparent glass. Not only does $CHCl_3$ improve the solubility of many precursors, but it leads to a higher yield of radical cations on radiolysis due to its ability to scavenge electrons by dissociative attachment ($CHCl_3 + e^- \rightarrow {}^{\bullet}CH_2Cl + Cl^-$).

The initial spectrum of ionized anthralin embedded in the above mixture shows only a very weak absorption at 700 nm (Figure 5, red trace). However, annealing of the matrix (up to 180 K) causes a significant growth of the anthralyl radical absorption (cf. blue lines). Juxtaposition of this spectrum to that obtained in MTHF (blue dashed line) and that obtained by depositing **(2)**$_2$ into an Ar matrix[51] indicates that the low energy shoulders at 740−800 nm are much weaker in the spectrum in the ionic liquids, a phenomenon for which we have no explanation. Although according to TD-DFT the absorptivity of **2**• at 700 nm is about 3 times greater than that of **1′**•+ (cf. Tables 3 and 4), the strong increase of the absorption at this wavelength indicates that **2**• cannot possibly be formed only at the expense of (i.e., by deprotonation of) **1′**•+. Thus, we presume that **2**• arises through reaction of **1** with radical byproducts of the radiolysis (analogous to reaction 2 in MTHF). At still higher temperature, the spectrum of the radical decays, too, leaving behind a species with an absorption at 440 nm.

3. Conclusions

Almost a century has elapsed since anthralin **1** was introduced as an antipsoriatic drug, but the mechanism by which **1** exerts its action on biological targets and the exact nature of the chemical species which are pharmacologically active has not yet been elucidated. In this paper, we presented for the first time the primary products of redox reactions involving **1**, i.e., its radical ions.

Addition of an electron to the **1** significantly increases its ability to act as a hydrogen atom donor. Although anthralin itself can lose a hydrogen atom in reactions with, e.g., peroxyl radicals, the extra electron diminishes the C(10)−H or C(10)−C(10′) bond dissociation energy in anthralin or its dimer, respectively.

A suprising finding of this study is that the anthralyl radical, **2**•, is much more reactive toward oxygen than the corresponding (closed shell) anion, **2**$^-$. Therefore, the direct auto-oxidation of **2**$^-$ cannot be responsible for the production of reactive oxygen species. Conversely, **2**• cannot be regarded as inactive toward oxygen.

Another surprising finding is that under conditions that usually lead to the formation of radical cations (X-irradiation in Ar doped with CH_2Cl_2), anthralin beats CH_2Cl_2 in scavenging the electrons that are liberated in the process and forms the radical anion. We plan to explore the scope of this method which allows in principle to record also the vibrational spectra of radical anions, something that, to the best of our knowledge, has not been tried to date.

4. Experimental Section

4.1. Materials. Anthralin, 2-chlorobutane, 2-methyltetrahydrofuran (MTHF), and chloroform were obtained from commercial sources. The anthralin dimer (1,8,1′,8′-tetrahydroxy-10,10′-bisanthrone) was prepared according to the procedure described previously.[43]

Preparation of 1-Butyl-3-methylimidazolium Hexafluorophosphate. A mixture of 1-methylimidazole (41 g, 0.5 mole) and 1-chlorobutane (47 g, 0.51 mole) was vigorously stirred and heated at 75 °C for 75 h. The resulting solid, 1-butyl-3-methylimidazolium chloride, was thoroughly washed with ethyl acetate (≥4 × 100 mL), and the remaining volatile compounds were removed by heating to 50 °C under 0.1 mmHg of pressure. To the chloride solution in 300 mL of water, cooled with an ice−water mixture and vigorously stirred, was added dropwise 160 g (0.65 mole) of 60% hexafluorophosphoric acid solution. The lower layer was separated and washed with deionized water until the washings were no longer acidic. The resulting yellowish viscous oil was dissolved in 150 mL of dichloromethane and purified on a chromatographic column packed with silica gel (15 g, lower) and charcoal (10 g, upper) layers. After the dichloromethane was removed on a rotavap, the remaining colorless oil was pumped at 0.1 mmHg/50 °C for 2 h to give 125 g (88%) of 1-butyl-3-methylimidazolium hexafluorophosphate.

4.2. Pulse Radiolysis. Pulse radiolysis experiments were carried out with high energy (6 MeV) 17 ns electron pulses generated from a linear electron accelerator. The dose absorbed per pulse was

(43) Auterhoff, H.; Scherff, F. C. *Arch. Pharm. (Weinheim)* **1960**, *293*, 918.
(44) Gebicki, J.; Marcinek, A.; Rogowski, J. *Radiat. Phys. Chem.* **1992**, *39*, 41.
(45) Karolczak, S.; Hodyr, K.; Lubis, R.; Kroh, J. *J. Radioanal. Nucl. Chem.* **1986**, *101*, 177.
(46) Marcinek, A.; Zielonka, J.; Gebicki, J.; Gordon, C. M.; Dunkin, I. R. *J. Phys. Chem. A* **2001**, *105*, 9305.
(47) Becke, A. D. *J. Chem. Phys.* **1993**, *98*, 5648.
(48) Lee, C.; Yang, W.; Parr, R. G. *Phys. Rev. B* **1988**, *37*, 785.
(49) Frisch, M. J.; et al. Gaussian 03, Rev B.01, Gaussian, Inc., Pittsburgh, 2003 (full reference given in Supporting Information).
(50) Casida, M. E. Time-Dependent Density Functional Response Theory for Molecules. In *Recent Advances in Density Functional Methods, Part I*; Chong, D. P., Ed.; World Scientific: Singapore, 1995; p 155.
(51) Ca. 135 °C are required to volatilize **(2)**$_2$. Under these conditions, the dimer appears to undergo partial dissociation before it is trapped in the Ar matrix.

http://doc.rero.ch

determined with an N_2O-saturated aqueous solution of KSCN (0.01 M), assuming $G((SCN)_2^{\bullet-}) = 6.0$ and $\epsilon((SCN)_2^{\bullet-}) = 7600\ M^{-1}\ cm^{-1}$ (G represents the yield of radicals per 100 eV of energy absorbed and ϵ is a molar extinction coefficient at 475 nm). The dose delivered per pulse was 5−80 Gy. The concentration of the solute was kept in the range of $(0.5-10) \times 10^{-3}$ M. Details of the pulse radiolysis system are given elsewhere.[44,45]

The radiolysis of 2-methyltetrahydrofuran leads to the formation of solvated electrons (e_{s-}) and the radical cations of solvent molecules (reaction 3).

$$C_5H_{10}O \rightarrow C_5H_{10}O^{\bullet+} + e_s^- \quad (3)$$

The solvated electrons react with the solute molecules (A) to give the corresponding *radical anions* (reaction 4), while the ionized solvent molecules easily transfer a proton onto neighboring neutral molecules (reaction 5).[22]

$$e_s^- + A \rightarrow A^{\bullet-} \quad (4)$$

$$C_5H_{10}O^{\bullet+} + C_5H_{10}O \rightarrow {}^{\bullet}C_5H_9O + C_5H_{11}O^+ \quad (5)$$

The products of this latter process can act as acids or as hydrogen atom donors/acceptors. Under matrix conditions these bimolecular reactions are, however, largely suppressed. They can be observed only upon softening of a matrix on its annealing.

For the attempted generation of *radical cations*, solutions of the anthralin in alkyl halides (2-chlorobutane or a 1:1 mixture of $CFCl_3$ and BrF_2C-CF_2Br) were used as these solvents dissociatively capture electrons ejected from the solvent molecules, while the positive charge is transferred to solute molecules of lower ionization potential.[22] Glassy matrices of 1-butyl-3-methylimidazolium hexafluorophosphate were used for the same purpose as this ionic liquid has proven suitable for the generation of radical cations.[46]

4.3. Cryogenic Measurements. Glassy samples of the MTHF, 2-chlorobutane, the above Freon mixture, or 1-butyl-3-methylimidazolium hexafluorophosphate/chloroform were prepared by immersing room-temperature solutions in liquid nitrogen in special cryogenic cuvettes. The samples were 0.5−3 mm thick and were placed in a optical dewar with liquid nitrogen or in a liquid nitrogen-cooled cryostat where any temperature between 77 and 150 K can be maintained by controlled heating. Ionization was effected by irradiation with 4 μs electron pulses from the linear accelerator (Lodz) or by irradiation in a ^{60}Co γ-source (Fribourg).

In the rare gas matrix isolation experiments[37] ground crystals of **1** or **(2)$_2$** were placed in heatable tube attached to the cryostat. From there they were evaporated very slowly at 65 (**1**) or 135 °C, respectively, for the dimer and co-deposited onto a CsI window held at 19 K with a 8:1 mixture of Ar and N_2 containing 1 mol % of CH_2Cl_2 (which acts as an electron scavenger). After taking reference spectra, the samples were exposed to 90 min of X-irradiation from a tungsten anode tube operated at 40 kV/40 mA.

4.4. Quantum Chemical Calculations. The geometries of all species were optimized by the B3LYP density functional method[47,48] as implemented in the Gaussian 03 suite of programs[49] using the 6-31G* basis set for neutral and cationic species, 6-31+G* for (radical) anions. Relative energies, including ZPE corrections, were calculated at the same levels.

Electronic transitions were predicted by density functional-based time-dependent response theory.[50] We used the formulation of TD-DFT implemented in the Gaussian 03 program,[49] together with the same functional and Gaussian basis sets as mentioned above.

Acknowledgment. This work was supported by grant from the Ministry of Science and Informatization (No. 4/*T*09A/020/24) and the Swiss National Science Foundation (project 200020-105217). We thank Prof. Jerzy Gebicki (Technical University of Lodz) for participation in the early stages of this project and for helpful discussions.

Supporting Information Available: Pictures of the orbitals involved in the electronic transitions of **1**$^{\bullet-}$, **2**$^-$, and **2**$^{\bullet}$ listed in Tables 1−3 and lowest energy pathway for the enolization of **1**$^{\bullet+}$. Cartesian coordinates and absolute energies, including thermal corrections, for all species discussed in this work from B3LYP calculations. This material is available free of charge via the Internet at http://pubs.acs.org.

http://doc.rero.ch